Journal of Applied Geophysics 104 (2014) 35–43

Contents lists available at ScienceDirect

Journal of Applied Geophysics

journal homepage: www.elsevier.com/locate/jappgeo

Incorporating ancillary data into the inversion of airborne time-domain electromagnetic data for hydrogeological applications

Vincenzo Sapia [a,*], Greg A. Oldenborger [b], Andrea Viezzoli [c], Marco Marchetti [a]

[a] Istituto Nazionale di Geofisica e Vulcanologia, Via di Vigna Murata 605, 00143, Rome, Italy
[b] Geological Survey of Canada, Natural Resources Canada, 601 Booth Street, Ottawa, ON, Canada
[c] Aarhus Geophysics Aps, C.F. Møllers Alle 4, Aarhus C 8000, Denmark

ARTICLE INFO

Article history:
Received 1 November 2013
Accepted 13 February 2014
Available online 20 February 2014

Keywords:
Airborne electromagnetics
Time domain electromagnetics
Hydrogeophysics
Data integration

ABSTRACT

Helicopter time-domain electromagnetic (HTEM) surveys often suffer from significant inaccuracies in the early-time or near-surface data—a problem that can lead to errors in the inverse model or limited near-surface resolution in the event that early time gates are removed. We present an example illustrating the use of seismic data to constrain the model recovered from an HTEM survey over the Spiritwood buried valley aquifer in Manitoba, Canada. The incorporation of seismic reflection surfaces results in improved near-surface resistivity in addition to a more continuous bedrock interface with a sharper contact. The seismic constraints reduce uncertainty in the resistivity values of the overlying layers, although no a priori information is added directly to those layers. Subsequently, we use electrical resistivity tomography (ERT) and borehole data to verify the constrained HTEM models. Treating the ERT and borehole logs as reference information, we perform an iterative time-shift calibration of the HTEM soundings to achieve regional-scale consistency between the recovered HTEM models and the reference information. Given the relatively small time-shifts employed, this calibration procedure most significantly affects the early-time data and brings the first useable time gate to a time earlier than the nominal first gate after ramp off. Although time shifts are small, changes in the model are observed from the near-surface to depths of 100 m. Calibration is combined with seismic constraints to achieve a model with the greatest level of consistency between data sets and, thus, the greatest degree of confidence. For the Spiritwood buried valley, calibrated and constrained models reveal more structure in the valley-fill sediments and increased continuity of the bedrock contact.

1. Introduction

The use of airborne geophysics for groundwater and other environmental and engineering applications has increased dramatically in the recent past due to advances in inversion and instrumentation. For example, airborne electromagnetics (AEM) have been applied increasingly to regional hydrogeological mapping (Jørgensen et al., 2003a; Møller et al., 2009; Oldenborger et al., 2013; Paine and Minty, 2005; Wynn, 2002). As a result of AEM improvements such as wider bandwidth, different coil configurations and increased sensitivity to small and shallow structures, the method has been adapted and employed for hydrogeological studies with the possibility to obtain quantitative information for groundwater applications (Viezzoli et al., 2010).

The advantages of airborne EM systems are rapid data acquisition, cost efficiency and high data density over large areas (Sapia et al., 2014). However, one limitation for most time-domain AEM systems is the inability to measure unbiased early-time voltage data for which timing and primary field removal are critical (Macnae and Baron-Hay, 2010). It is these early-time data that provide the very near-surface sensitivity, which is a crucial part of groundwater applications. Furthermore, the design of AEM systems is complex, and the acquisition of AEM data can be affected by a number of noise sources both internal and external to the system. For example, the definition of an absolute time-zero can be problematic in addition to transmitter–receiver synchronization (Christiansen et al., 2011). With the objective of increased near-surface resolution, advancements have been made in AEM system design (Sørensen and Auken, 2004; Sørensen and Nyboe, 2012), system modeling (Christiansen et al., 2011) and through AEM survey calibration based on ancillary information (Auken et al., 2009; Foged et al., 2013; Podgorski et al., 2013). In addition, the joint interpretation of high-resolution seismic data and AEM inversions has been performed to enhance AEM results with different levels of detail (Gabriel et al., 2003; Høyer et al., 2011; Jørgensen et al., 2003b; Oldenborger et al., 2013). Electrical resistivity tomography (ERT) results have been used to support AEM interpretations within a coal-waste impoundment (Hammack et al., 2010), for uranium deposits (Smith et al., 2011), for coastland investigations (Viezzoli et al., 2010) and for an abandoned salt mine (Siemon et al., 2012). Such comparisons of

* Corresponding author at: Istituto Nazionale di Geofisica e Vulcanologia, Via della Grande Muraglia 605, 00144, Rome, Italy. Tel.: +39 0651860723.
E-mail address: vincenzo.sapia@ingv.it (V. Sapia).

http://dx.doi.org/10.1016/j.jappgeo.2014.02.009
0926-9851/

results from different survey types, in effort to support the geological interpretation, are not the same as integrating different data types in a single inversion process. Burschil et al. (2012) present a study where picked horizons from several seismic lines were applied as a priori information to layer boundaries, leading to more reliable resistivity models of the subsurface.

In this paper, we investigate how data integration (combination of several complimentary types of geophysical data) can improve inversions, reduce ambiguity and deliver high-resolution results for the very near surface. We examine the benefit of incorporating ancillary seismic data and ERT results into the inversion of helicopter time-domain electromagnetic (HTEM) data collected over the Spiritwood buried valley aquifer in Manitoba, Canada. Reflection surfaces picked from high-resolution seismic reflection data are used as a priori information to define layer depths in the inversion of HTEM data. This leverages the high-resolution architectural nature of the seismic data against the material property sensitivity of the HTEM data and results in consistency between the data sets but does not necessarily yield an inversion result that is in agreement with geological knowledge. To this end, we also devise a calibration method for HTEM data using ERT models as reference information. The quantitative application of ERT models as constraint information is not as straightforward as for the seismic data since layer boundaries are not well defined from ERT. Alternatively, our calibration is an iterative procedure that involves applying small pre-inversion time shifts to the HTEM soundings; the appropriate time shift is chosen as the one that provides the best post-inversion match between the HTEM and the ERT models. The result is a model that benefits from the near-surface resolution of the ERT and a methodology that can be applied to the entire HTEM survey area.

2. Study area and methods

The Spiritwood aquifer is a Canada–USA trans-border buried valley aquifer that runs approximately NW–SE and extends 500 km from Manitoba, across North Dakota and into South Dakota (Betcher et al., 2005; Winter et al., 1984). The Spiritwood aquifer system consists of a broad north–south trending shale bedrock valley filled with glacially deposited silt and clay diamicton with sand and gravel bodies (Randich and Kuzniar, 1984; Wiecek, 2009). Within the broad Spiritwood valley are a series of narrow inset valleys with complex geometry (Oldenborger et al., 2013). Several geophysical and geological data sets have been collected over the Spiritwood (Crow et al., 2012; Oldenborger, 2010a, 2010b; Pugin et al., 2011), making it a good candidate for survey comparisons, data integration and calibration studies. Versatile time domain electromagnetic (VTEM) data were collected by Geotech, Ltd. over the Spiritwood using a newly developed full waveform system designed for obtaining improved early-time data and shallow imaging capability (Legault et al., 2012). The VTEM transmitter pulse shape is trapezoidal with a base frequency of 30 Hz and nominal 4.073 ms pulse width. Forty-four time measurement gates are used for the final data in the range of 0.018–9.977 ms. Pre-processing by Geotech included streamed half-cycle system calibration, drift corrections, parasitic noise corrections and ideal waveform deconvolution (Legault et al., 2012; Macnae and Baron-Hay, 2010). After calibration and deconvolution, digital filtering was used to reject major sferic events and to reduce noise levels.

The Spiritwood VTEM survey consists of three separate blocks of closely spaced lines (300 m separation) that cover approximately 220 line km in regions of existing seismic, electrical and borehole data. We focus on two profiles in the north and the south of the survey area (S2007 and S1, Fig. 1).

Inversions of the VTEM data along S2007 and S1 are carried out using quasi 3D Spatially Constrained Inversion (SCI; Viezzoli et al., 2008). Prior to inversion, navigation data are filtered and averaged automatically, and additional manual corrections are applied to the altitude data to remove outliers (e.g., Jørgensen et al., 2013). Data are

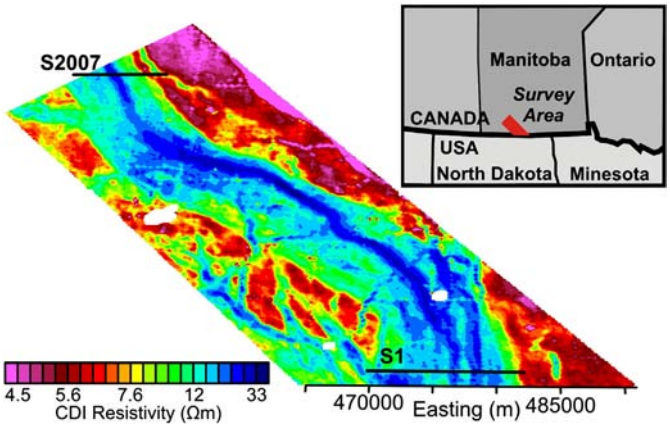

Fig. 1. Map of the Spiritwood aquifer survey area and a conductivity depth image (CDI) at 70 m depth illustrating buried valley morphology (Oldenborger et al., 2013). VTEM data were collected along the northern and southern seismic lines shown in black (S2007 and S1, respectively). (For interpretation of the references to colour in this figure, the reader is referred to the web version of this article.)

filtered for coupling or noise due to the presence of culture. Data are then averaged spatially using trapezoid filters that allow enhanced signal to noise levels at late time without compromising lateral resolution at early time (Auken et al., 2009). Soundings were taken each 1.5 s, which corresponds to approximately 30 m along a flight line. During inversion, the flight altitude is treated as an inversion parameter, and the depth of investigation (DOI) is calculated for the output models (Christiansen and Auken, 2012). The inversion is parameterized with 29 layers with logarithmically increasing thickness to a depth of 200 m with a homogeneous half space of 40 Ωm as a starting model.

Preliminary inversions of the VTEM data resulted in a strong, thin conductor at the surface of the model. Such a conductor was not expected for the given geological setting. Inspection of the predicted data revealed poor fits for the first two data gates (Fig. 2). Our results suggest an initial transient amplitude that is inconsistent with the forward model. This discrepancy could be attributed to a number of factors including incomplete primary field decay or incorrect AEM system description. Christiansen et al. (2011) describe in detail the effect of inaccurate modeling of the system transfer function in model space. Errors in the description of the system transfer function influence the inverted model differently at the early and late times; the output model can differ quite dramatically from the true model, and the measured data are sometimes not fit within the noise level. Regardless of cause, we have an early-time signal bias that cannot be accounted for. Therefore, the first two gates (21 μs and 26 μs after ramp off) are omitted from all subsequent inversions and early-time noise levels are doubled for gate centers earlier than 40 μs.

2.1. Ancillary data

A ground-based geophysical campaign for the Spiritwood provided over 10 km of electrical resistivity data and over 40 km of land streamer seismic reflection data (Oldenborger et al., 2013). To provide additional information and, in particular, some independent measurements of subsurface resistivity values, a ground electrical resistivity survey program was also conducted (Oldenborger et al., 2013). Electrical resistivity data were collected along S2007 using a Multi-Phase Technologies DAS-1 system with 64-electrode dipole-dipole geometry. The data were inverted using the smoothness-constrained least-squares algorithm of Loke et al. (2003) with depth of investigation estimated following Oldenburg and Li (1999). The ERT model in Fig. 3a exhibits a very narrow range of resistivity (5–45 Ωm). Nevertheless, we clearly identify the conductive basement (below 10 Ωm), the resistive incised valley fill (above 30 Ωm) and the heterogeneous intermediate till package overlying bedrock.

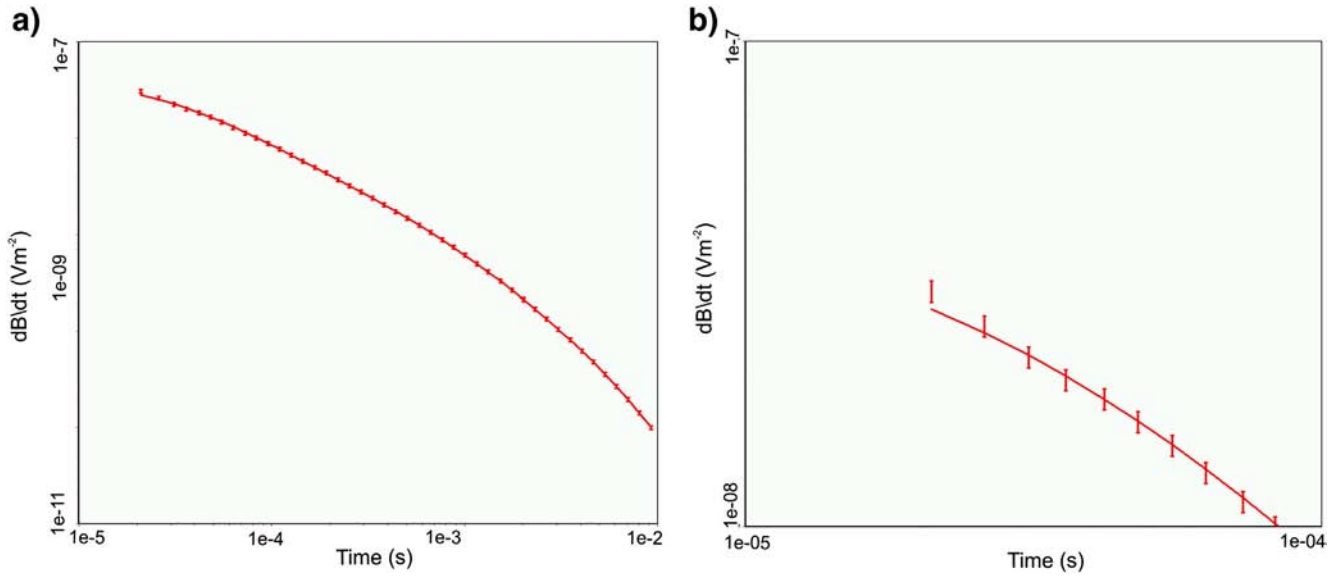

Fig. 2. Example of unconstrained VTEM decay curve and data fit. (a) VTEM forward response (solid line) and all measured time gates (vertical bars). (b) Early-time portion of the decay curve showing the misfit at gates 1 and 2 at 21 μs and 26 μs after the end of the ramp off. (For interpretation of the references to colour in this figure, the reader is referred to the web version of this article.)

The seismic reflection methodology is described in detail by Pugin et al. (2009), and Spiritwood reflection sections are discussed by Pugin et al. (2011). The data were collected with a vibratory source both in horizontal and vertical mode using a sweep of 20–240 Hz; 48 three-component geophones were arranged as a land streamer at 1.5 m spacing. Only the compressional-wave data are considered for this work. Fig. 3a shows the P-wave seismic reflection data along with the ERT model along section S2007; Fig. 3b shows the P-wave reflection data along with a cored borehole along section S1 (Crow et al., 2012; Oldenborger et al., 2013). The solid black lines identify the bedrock surface interpreted from a significant change in reflection facies. Several valley features are apparent in the bedrock topography that can be correlated with resistive fill along S2007. The dashed black line (Fig. 3b) identifies a reflector attributed to a shallow inter-till transition between a heterogeneous, less compact surficial till and an underlying more compact till. The same inter-till boundary may correspond to the resistive surface layer observed in the S2007 ERT data, but it is not as apparent in the S2007 seismic reflection character.

3. Results

Inversion results for the gate-edited VTEM data along section S2007 are show in Fig. 4a. In general, the VTEM result is in good agreement with supporting data in terms of depth of the conductive shale bedrock.

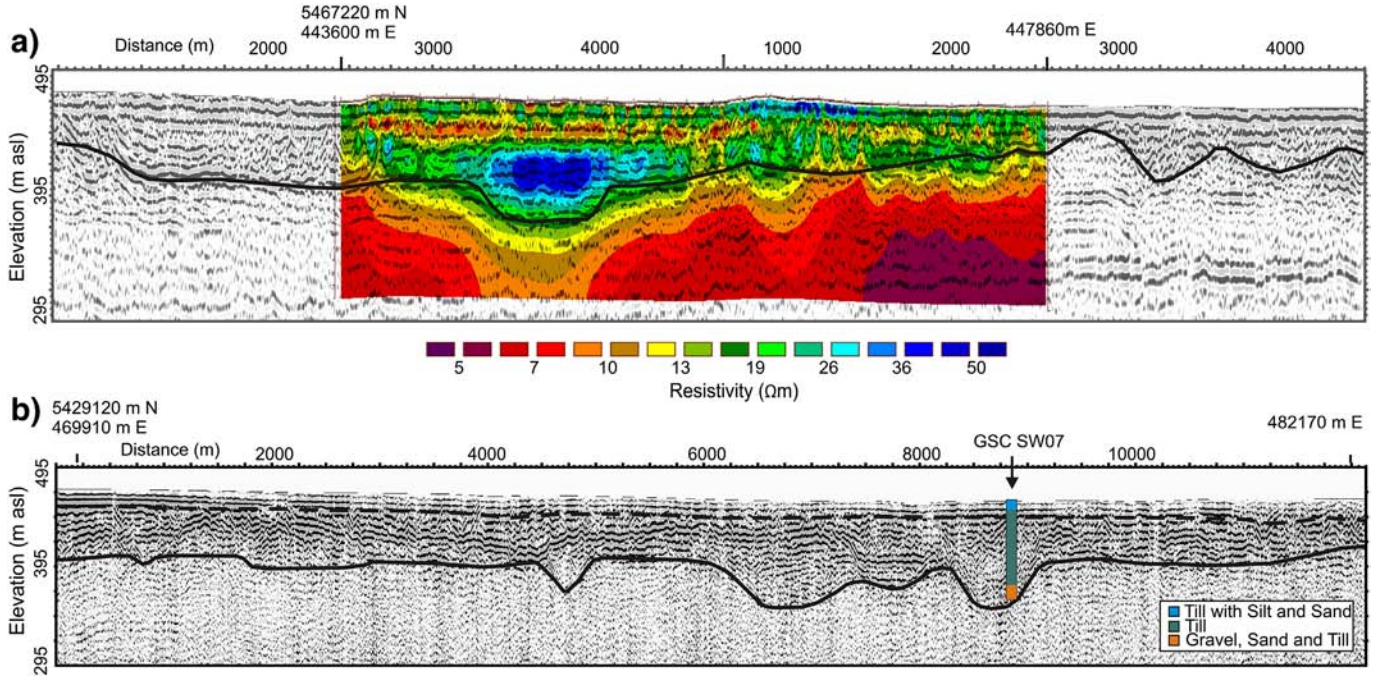

Fig. 3. Seismic and electrical data for the Spiritwood aquifer survey area. (a) Northern profile S2007 with P-wave reflection section and ERT model. RMS misfit on the S2007 ERT inversion is 3%. (b) Southern profile S1 with P-wave reflection section and cored borehole GSC-SW-07. Solid black lines represent the interpreted bedrock reflection surface; dashed black line represents interpreted inter-till reflection surface. (For interpretation of the references to colour in this figure, the reader is referred to the web version of this article.)

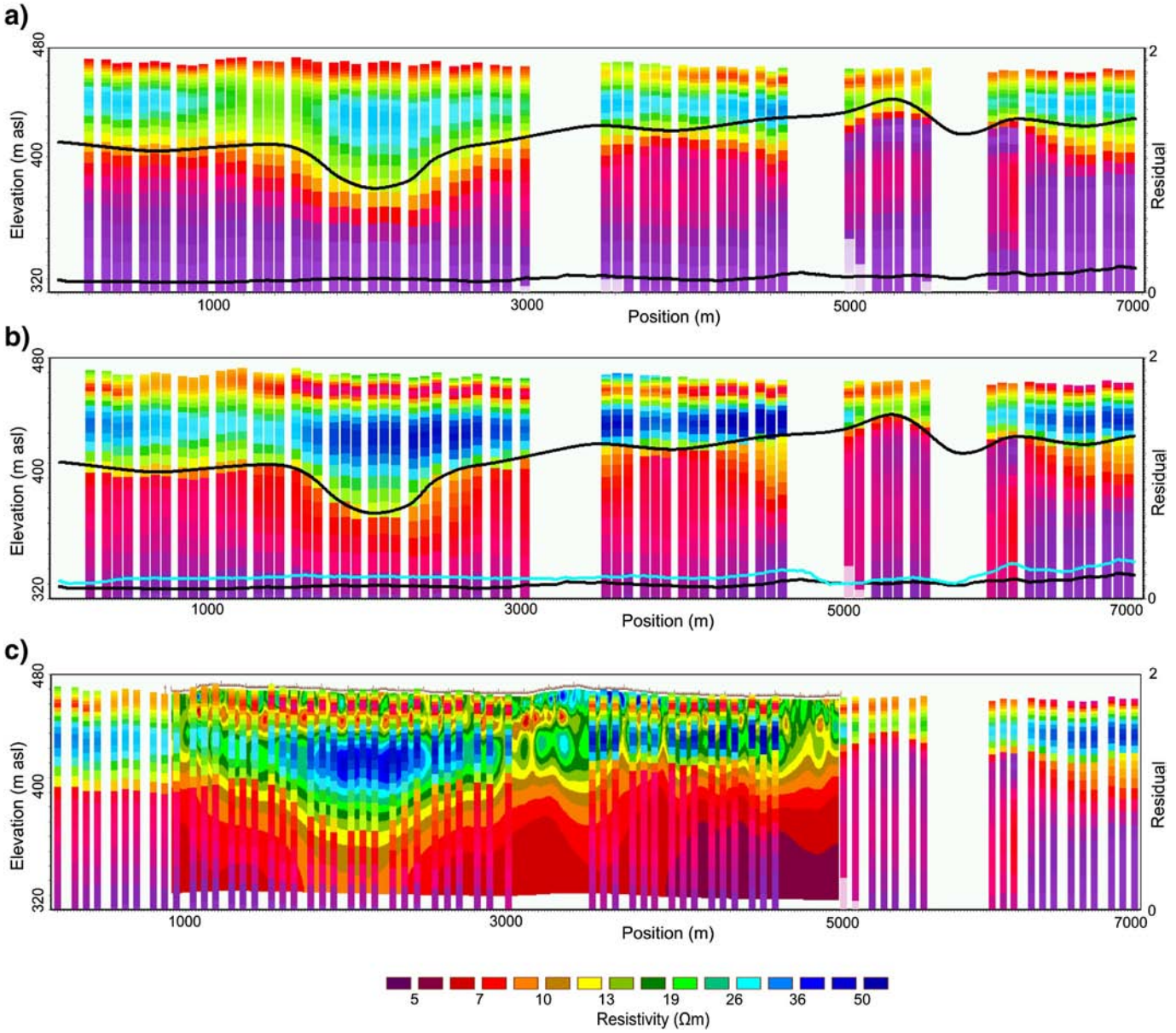

Fig. 4. S2007 VTEM inversion results. (a) Unconstrained. Upper solid black line is the bedrock reflection surface. Lower solid black line is the unconstrained data residual or misfit. (b) Constrained with bedrock reflection surface and bedrock conductivity of 7 Ωm (standard deviation factor of 1.5). Solid blue line is the constrained data residual. (c) Comparison of ERT model with the constrained VTEM model. The VTEM model underestimates the depth to the shallow conductive layer by approximately 10 m. (For interpretation of the references to colour in this figure, the reader is referred to the web version of this article.)

However, the SCI suffers from the overestimation of depth to bedrock. Compared to the ERT model, the VTEM model clearly resolves the resistive body filling the incised valley as well as the conductive shale bedrock. However, significant discrepancies exist in the near surface where the VTEM model lacks a continuous resistive surface layer. To improve the model, we add the seismic data to the inversion using the SCI framework for which constraints represent a priori information that are fit together with the VTEM data during the inversion. The seismic data are used as a source of ancillary information on the elevation of the contact between the resistive infill materials and the conductive bedrock. The a priori constraints also consist of a resistivity value to be associated with the bedrock layer along with a defined standard deviation. A histogram analysis of the unconstrained model yields a peak resistivity of approximately 7 Ωm, which we utilize as the shale bedrock resistivity.

Constrained inversion results along section S2007 are shown in Fig. 4b. As a result of the constraint, we see that not only is the bedrock contact sharper, but also a resistive surface layer is more discernible. The data residual is computed as the mean squared difference, weighed against noise level; after the application of constraints, the residual doubles but remains well within the gate dependent noise levels assigned to the soundings indicating that the a priori information is consistent with the VTEM data. However, the near-surface structure is still significantly different from that suggested by the ERT (Fig. 4c). In particular, the shallow transition from a resistive surface to a conductive layer occurs at too shallow a depth, and the incised valley fill is not readily distinguished from the surrounding overburden. When we examine the soundings, we see that the VTEM data are consistently under-predicted at times less than approximately 80 μs (Fig. 5).

To reduce this early-time data misfit, we consider calibrating the S2007 VTEM data using the ERT as an iterative model-space constraint. We apply incremental negative time shifts to the VTEM data gates and invert the shifted data until we obtain an optimum level of fit between the resulting VTEM model resistivity and the ERT model resistivity. This

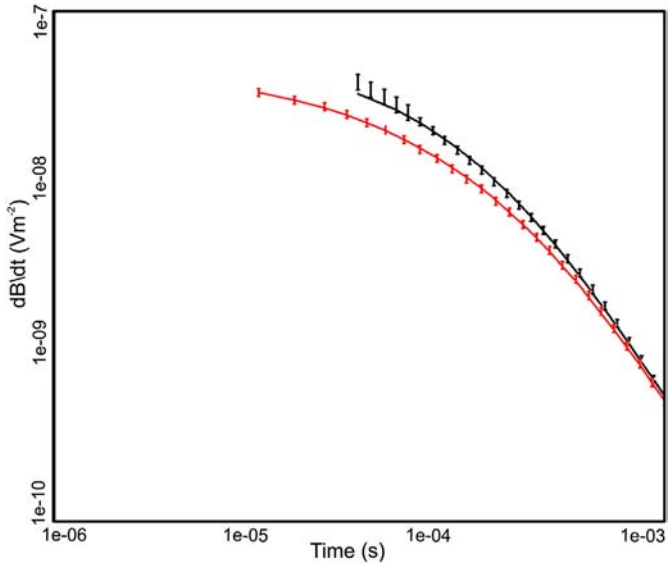

Fig. 5. Example of constrained VTEM decay curves and data fit before (black) and after the calibration (red). Despite increased noise levels for the first 5 gates, the forward model gives a poor fit to the uncalibrated data at early time (black). After calibration by −21 μs, the forward model fits the data well without increasing the noise level of the time gates (red). (For interpretation of the references to colour in this figure, the reader is referred to the web version of this article.)

procedure is similar to the data space calibrations described by Foged et al. (2013) and Podgorski et al. (2013), which may be applicable when high-quality ground TEM data are available. However, ground TEM surveys and AEM surveys represent compatible data types that can be directly compared. This is not the case for AEM and ERT data, although the models should be directly comparable provided that effects of anisotropy and scale are negligible.

For section S2007, we find an optimal time shift of −21 μs that is applied to all VTEM gate times. This brings the first usable data gate (corresponding to the nominal third gate) to a time of 10 μs after the end of the ramp off. (Recall that the VTEM nominal gates 1 and 2 have been omitted from all inversions.) After the inversion of the calibrated data, the VTEM model is in better agreement with the ERT model across the S2007 section (Fig. 6a). The surface shows up as a resistive feature, and the resistive anomaly associated with the valley fill is well delineated. These features are of significant hydrogeological influence in terms of governing the recharge pathway from the surface and the aquifer potential of the buried valley. The inversion of the calibrated data can also be constrained with seismic depth to bedrock in the model space. The outcome is a sharper bedrock surface and more subtle changes in the resistivity structure of the valley fill (Fig. 6b and c).

We perform the same procedure for section S1 in the south part of the survey block, and the results are shown in Fig. 7. The unconstrained inversion of the S1 VTEM data results in a clear depiction of the conductive shale bedrock, the buried valley morphology, and the heterogeneous overburden material (Fig. 7a). However, as with section S2007, the unconstrained model suffers from main incised valleys that appear deeper than the interpreted seismic bedrock depth. The unconstrained model also exhibits a conductive surface layer that appears to coincide well with the identified inter-till reflection. However, the ERT models from across the survey area and the electromagnetic log from borehole GSC SW07 (Fig. 3) all suggest a moderately resistive surface layer (Crow et al., 2012; Oldenborger et al., 2013).

The overestimation of the depth to bedrock might be due to several factors. The incised valleys are narrow structures that have the potential for 2D/3D effects on the 1D inversion (Goldman et al., 1984). Furthermore, the seismic data depict reflection surfaces in terms of changes in elastic moduli. However, the till/bedrock interface may not be uniquely defined in terms of both seismic parameters and electrical resistivity; the resistivity may vary gradually across the sediment/bedrock interface and even a sharp electrical contact will be subject to smoothing conditions of the inversion (Auken and Christiansen, 2004).

To reduce ambiguity of the model, we constrain the VTEM inversion with the interpreted seismic bedrock reflection surface; the result is shown in Fig. 7b. In addition to controlling the depth to the conductive bedrock, the constraint results in a general increase in overburden resistivity and the emergence of a resistive surface layer. However, the resistive surface layer appears too thin and correspondence with seismic reflector is limited.

To further refine the VTEM model, we apply the calibration time shift determined for section S2007. Fig. 8a shows the calibrated inversion result without any seismic constraint. The calibrated result clearly shows a resistive surface layer approximately 10 m thick that corresponds to the shallow seismic reflector. However, the calibrated results still lack good discrimination of the valley-fill sediments, and there is some discrepancy between the deep conductive layer and the interpreted bedrock topography. When we combine the time-shift calibration with the seismic bedrock constraint, we obtain more structure in the valley-fill sediments and increased consistency of the bedrock contact (Fig. 8b). Constraining to seismic data has the expected effect of creating a sharp bedrock contact, but it also results in changes to the resistivity structure of the overburden to which no a priori constraint was explicitly applied. There is still some overestimation of depth to the strong conductor beneath the incised channels and this may be due to 3D effects or loss of signal and resolution.

4. Discussion

The inversion of noisy, band-limited AEM data is inherently ill posed, and results are notoriously non-unique (Ellis, 1998). Nevertheless, we would like to use the VTEM inversion results to build geological and hydrogeological models including the near surface. To this effect, we have utilized ancillary information to impose a priori constraints in model space and to perform the calibration of VTEM data such that inversion results are consistent with other information and data types.

Seismic data provide high-resolution information regarding changes in seismic velocity that are used to derive an independent measure of depth to model layers such as the conductive shale bedrock. For the Spiritwood VTEM data, seismic constraints provide improved results, particularly in resolving depth to bedrock at the bottom of buried valleys. Results are further improved via the calibration of the VTEM resistivity model against an electrical resistivity model derived from ERT and borehole data. In this way, we leverage the higher resolution and complimentary sensitivities of the seismic and electrical data to achieve a final VTEM model with a higher degree of confidence.

Our time-shift calibration is similar to that applied for ground-based TEM data and HTEM data by Foged et al. (2013) and Podgorski et al. (2013) but is more generally applicable to ancillary information that is not directly comparable in data space. Our calibration focuses on the 2D cognitive comparison of resistivity magnitude, structures and features in model space for an entire flight profile. This approach ameliorates some issues associated with discrepancies in support volume and resolution/regularization between data types and model derivations that may be variable across a test section. We consider the model-space calibration as an appropriate way to integrate electrical and AEM methods or other reference information that is not directly transferable to AEM data space. However, it is of utmost importance to honor the quality of the calibration reference information and the validity of the model-to-model comparison since any errors may be propagated to the calibrated AEM.

For ERT and AEM models, we have inherent differences in the survey methods, acquisition procedures, measured data, noise levels and support volume of measurement. Although both methods respond to the electrical conductivity of the subsurface, they sample significantly different

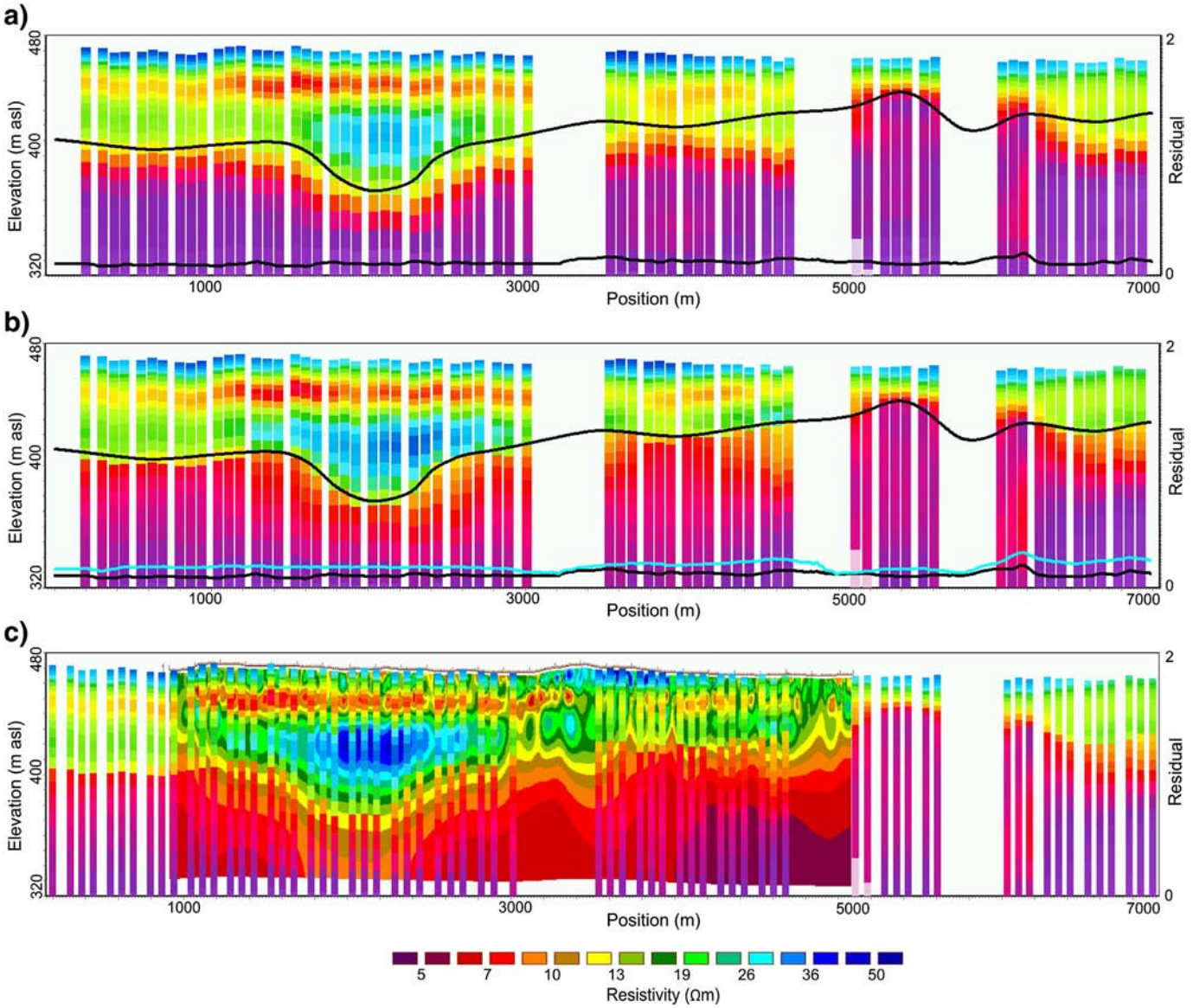

Fig. 6. S2007 calibrated VTEM inversion results. (a) Calibrated and unconstrained. Upper solid black line is the bedrock reflection surface. Lower solid black line is the unconstrained data residual or misfit. (b) Calibrated and constrained with bedrock reflection surface. Solid blue line is the constrained data residual. (c) Comparison of ERT model with the calibrated and constrained VTEM model showing significantly improved agreement. (For interpretation of the references to colour in this figure, the reader is referred to the web version of this article.)

volumes and have different sensitivities (geometry-based versus frequency-based). AEM has an area of investigation that is a function of the descending and expanding image of the transmitted current. The ERT method samples a portion of the ground defined by the region of galvanic current injection. Moreover, high-resistivity structures cannot be resolved easily using inductive methods, whereas they are better resolved by ERT. In theory, the inversion acts to remove differences between data types and data geometry (i.e., current patterns and sensitivity) to the limit of macro-anisotropy (Christensen, 2000) such that output models can be taken to be the representations of the physical parameter within some limitations such as resolution and regularization. Even a joint inversion should not require any corrections for anisotropy of scale—that is, anisotropy that is due to features of resolvable size (e.g., Monteiro Santos and El-Kaliouby, 2011; Raiche et al., 1985).

The surficial sediments in the Spiritwood region are largely carbonate-rich silty-to-sandy diamicton (till) with localized glaciofluvial deposits. Given the unsorted nature of the diamicton, we do not expect anisotropy associated with large-scale clay fabric. However, discrete clay layers, sand lenses or till fabric may influence the electrical anisotropy (Sutinen et al., 2010). The borehole GSCSW07 along section S1 (Fig. 3) intercepts the surficial sandy-till layer that we attribute to be the source of the resistive surface layer observed in ERT profiles across the survey area (Oldenborger et al., 2013). From the electromagnetic log of GSCSW07 (Crow et al., 2012), we extract an estimate of horizontal resistivity for this 10-m-thick surficial layer of $\rho_H \approx 15\ \Omega m$. From the ERT models, we estimate a bulk resistivity of $\rho \approx 18–23\ \Omega m$, although there is a significant degree of heterogeneity. These approximate resistivities suggest at least some degree of anisotropy with vertical resistivities of $\rho_V \approx 21–35\ \Omega m$. While significant, this degree of anisotropy would not significantly affect our calibration due to the cognitive nature of the model comparison that involves visually observing the degree of match between models in terms of both resistivity magnitude and structure over the entire 2D profile. Our calibration will be robust with respect to relatively small differences in model resolution, model errors or artifacts, but it can also be performed to different levels of stringency in the face of uncertainty. For example, a minimum requirement for the calibration of the Spiritwood VTEM data might be that it results in the structure of resistor over conductor over resistor over bedrock,

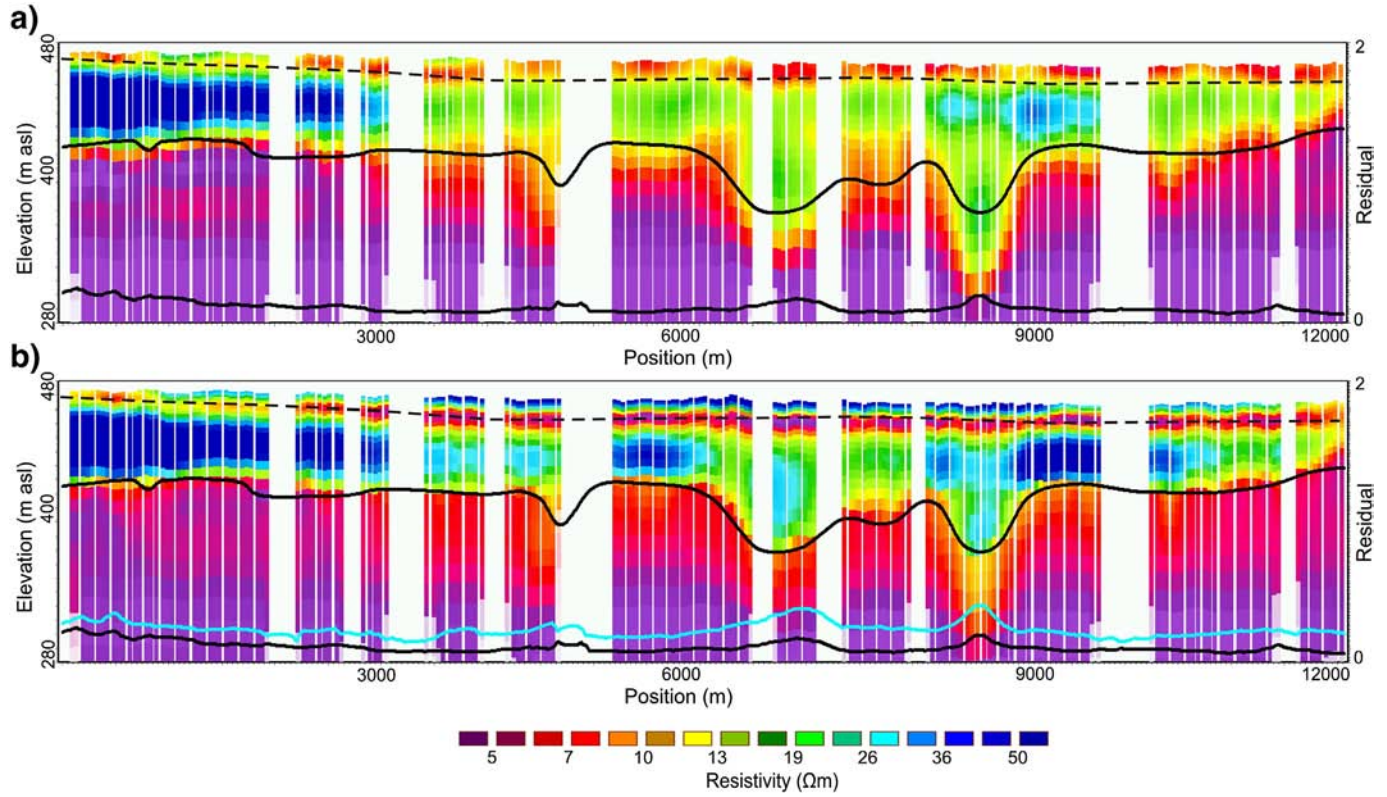

Fig. 7. S1 VTEM inversion results. (a) Unconstrained. Dashed black line is the inter-till reflection surface. Upper solid black line is the bedrock reflection surface. Lower solid black line is the unconstrained data residual or misfit. (b) Constrained with bedrock reflection surface. Solid blue line is the constrained data residual. (For interpretation of the references to colour in this figure, the reader is referred to the web version of this article.)

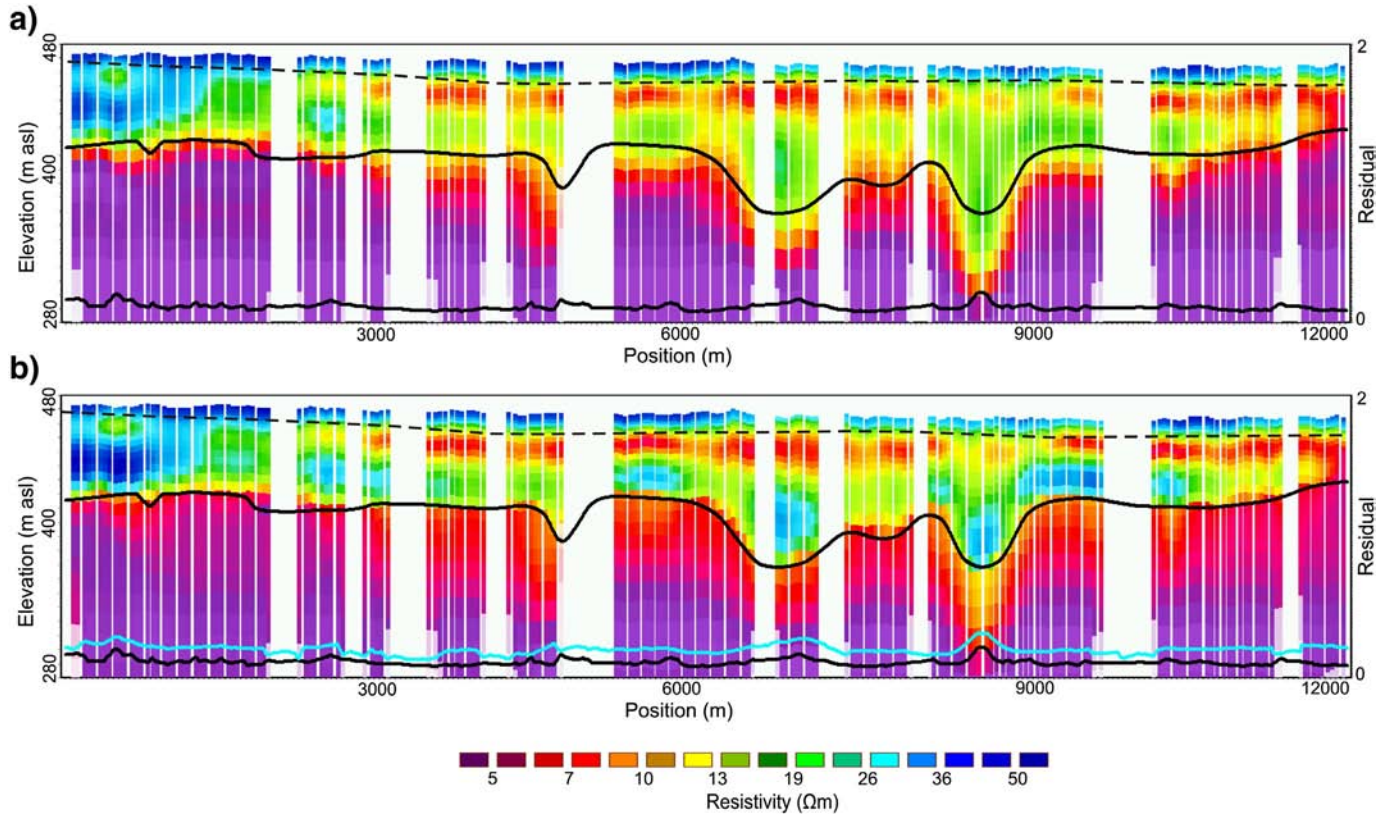

Fig. 8. S1 calibrated VTEM inversion results. (a) Calibrated and unconstrained. Lower solid black line is the unconstrained data residual or misfit. (b) Calibrated and constrained with bedrock reflection surface. Solid blue line is the constrained data residual. (For interpretation of the references to colour in this figure, the reader is referred to the web version of this article.)

as opposed to the structure observed with no calibration of conductor over resistor over bedrock.

Our calibration procedure was designed to reconcile early-time signal bias observed in the VTEM soundings that could not be accounted for in our forward modeling, but it does not require identification of the source of this bias. We hypothesize that signal bias most likely results from a large amount of primary field impacting the received signal at early times as a result of imprecision in timing, turnoff and establishment of time zero with respect to the transmitter waveform. However, neither the fact that our calibration empirically improves the fit between the observed data and our 1D forward model nor the observation that inversion results are in better agreement with ancillary information are conclusive evidence of a "timing error" in the data. We may have additional system effects such as current leaks or parasitic capacitance that contribute to enhanced signal strength at early time, or we may have modeling deficiencies (such as anisotropy) that result in underprediction of the true signal strength. Of particular note is that the time-shift calibration established for one part of our survey region is successfully applied to another in terms of agreement with other available data. This may not always be the case and the appropriate time shift is likely different for other systems and may be different for different data sets or flights with the same system.

5. Conclusion

In hydrogeological applications with multi-scale and complex aquifer systems such as glacial buried valleys, aquifer mapping requires the ability to accurately resolve aquifer geometry and to distinguish physical properties or aquifer materials. For example, bedrock or aquitard depth is an important starting point for exploitation drilling or groundwater modeling. However, an aquifer is also characterized by permeable sediments, which may have a distinct signature in terms of electrical resistivity.

We have demonstrated a two-part procedure that aims to build a resistivity model from the inversion of HTEM data by incorporating ancillary information from seismic and ERT data sets. Seismic data provide model-space constraints that result in a better recovery of valley bottoms and a more continuous bedrock surface. ERT models are used in an iterative calibration that involves incremental time shifts to the data gates and post-inversion model-to-model comparison. Calibration results in significant changes to the structure of the recovered HTEM model such that it is consistent with all available sources of information.

Our procedure is pragmatic and results based in that sources of noise in the data or sources of artifacts or deficiencies in the model need not be identified. By applying the calibration to an entire data set, the advantages of the regional extent and high spatial density of AEM can be fully utilized. Consistency across data types results in increased confidence in the resistivity model that is critical for groundwater mapping or hydrogeological model building on which management decisions are based. An important corollary is that the constrained and calibrated HTEM results will be of a quality commensurate with the ancillary information.

Acknowledgments

We are grateful to Geotech Ltd. for providing the processed VTEM data and to A. Pugin for providing the seismic data and interpreted reflection surfaces and helpful discussion. This work is part of the Groundwater Geoscience Program, Natural Resources Canada.

References

Auken, E., Christiansen, A.V., 2004. Layered and laterally constrained 2D inversion of resistivity data. Geophysics 69, 752–761. http://dx.doi.org/10.1190/1.1759461.

Auken, E., Christiansen, A.V., Westergaard, J.H., Kirkegaard, C., Foged, N., Viezzoli, A., 2009. An integrated processing scheme for high-resolution airborne electromagnetic surveys, the SkyTEM system. Explor. Geophys. 2009 (40), 184–192. http://dx.doi.org/10.1071/EG08128.

Betcher, R.N., Matille, G., Keller, G., 2005. Yes Virginia, there are buried valley aquifers in Manitoba. Proceedings of the 58th Canadian Geotechnical Conference, 6E-519.

Burschil, T., Wiederholda, H., Auken, E., 2012. Seismic results as a-priori knowledge for airborne TEM data inversion—a case study. J. Appl. Geophys. 80, 121–128. http://dx.doi.org/10.1016/j.jappgeo.2012.02.003.

Christensen, N.B., 2000. Difficulties in determining electrical anisotropy in subsurface investigations. Geoph. Prosp. 48, 1–19.

Christiansen, A.V., Auken, E., 2012. A global measure for depth of investigation. Geophysics 77, 171–177. http://dx.doi.org/10.1190/geo2011-0393.1.

Christiansen, A.V., Auken, E., Viezzoli, A., 2011. Quantification of modeling errors in airborne TEM caused by inaccurate system description. Geophysics 76, 43–52. http://dx.doi.org/10.1190/1.3511354.

Crow, H.L., Knight, R.D., Medioli, B.E., Hinton, M.J., Plourde, A., Pugin, A.J.-M., Brewer, K.D., Russell, H.A.J., Sharpe, D.R., 2012. Geological, hydrogeological, geophysical, and geochemistry data from a cored borehole in the Spiritwood buried valley, southwest Manitoba. Geological Survey of Canada (Open File 7079).

Ellis, R.G., 1998. Inversion of airborne electromagnetic data. Explor. Geophys. 29, 121–127. http://dx.doi.org/10.1071/EG998121.

Foged, N., Auken, E., Christiansen, A.V., Sørensen, K.I., 2013. Test site calibration and validation of airborne and ground based TEM systems. Geophysics 78, 95–106. http://dx.doi.org/10.1190/geo2012-0244.1.

Gabriel, G., Kirsch, R., Siemon, B., Wiederhold, H., 2003. Geophysical investigation of buried Pleistocene subglacial valleys in Northern Germany. J. Appl. Geophys. 53, 159–180. http://dx.doi.org/10.1016/j.jappgeo.2003.08.005.

Goldman, M., Tabarovsky, L., Rabinovich, M., 1984. On the influence of 3-D structures in the interpretation of transient electromagnetic sounding data. Geophysics 59, 889–901. http://dx.doi.org/10.1190/1.1443648.

Hammack, R., Kaminski, V., Harbert, W., Veloski, G., Lipinski, B., 2010. Using helicopter electromagnetic (HEM) surveys to identify potential hazards at coal-waste impoundments: examples from West Virginia. Geophysics 75, 221–229. http://dx.doi.org/10.1190/1.3505764.

Høyer, A.S., Lykke-Andersen, H., Jorgensen, F., Auken, E., 2011. Combined interpretation of SkyTEM and high-resolution seismic data. Phys. Chem. Earth 36, 1386–1397. http://dx.doi.org/10.1016/j.pce.2011.01.001.

Jørgensen, F., Møller, R.R., Nebel, L., Jensen, N.-P., Christiansen, A.V., Sandersen, P.B.E., 2013. A method for cognitive 3D geological voxel modelling of AEM data. Bull. Eng. Geol. Environ. 72, 421–432.

Jørgensen, F., Sandersen, P.B.E., Auken, E., 2003a. Imaging buried Quaternary valleys using the transient electromagnetic method. J. Appl. Geophys. 53, 199–213. http://dx.doi.org/10.1016/j.jappgeo.2003.08.016.

Jørgensen, F., Andersen, H.L., Sandersen, P., Auken, E., Nørmark, E., 2003b. Geophysical investigations of buried valleys in Denmark: an integrated application of transient electromagnetic and reflection seismic surveys, and exploratory well data. J. Appl. Geophys. 53, 215–228. http://dx.doi.org/10.1016/j.jappgeo.2003.08.017.

Legault, J.M., Prikhodko, A., Dodds, D.J., Macnae, J.C., Oldenborger, G.A., 2012. Results of recent VTEM helicopter system development testing over the Spiritwood Valley aquifer, Manitoba. 25th Symposium on the Application of Geophysics to Engineering and Environmental Problems (SAGEEP), Tucson, Arizona, USA.

Loke, M.H., Acworth, I., Dahlin, T., 2003. A comparison of smooth and blocky inversion methods in 2D electrical imaging surveys. Explor. Geophys. 34, 182–187. http://dx.doi.org/10.1071/EG03182.

Macnae, J., Baron-Hay, S., 2010. Reprocessing strategy to obtain quantitative early-time data from historic VTEM surveys. 21st International Geophysical Conference & Exhibition, ASEG, Sydney, Australia.

Møller, I., Søndergaard, V.H., Jørgensen, F., Auken, E., Christiansen, A.V., 2009. Integrated management and utilization of hydrogeophysical data on a national scale. Near Surf. Geophys. 7, 647–659. http://dx.doi.org/10.3997/1873-0604.2009031.

Monteiro Santos, F.A., El-Kaliouby, H.M., 2011. Quasi-2D inversion of DCR and TDEM data for shallow investigations. Geophysics 76, 239–250. http://dx.doi.org/10.1190/1.3587218.

Oldenborger, G.A., 2010a. AeroTEM III Survey, Spiritwood Valley, Manitoba, parts of NTS 62G/3, 62G/4, Manitoba. Geological Survey of Canada (Open File 6663).

Oldenborger, G.A., 2010b. AeroTEM III Survey, Spiritwood Valley, Manitoba, parts of NTS 62G/3, 62G/4, 62G/5, 62G/6, Manitoba. Geological Survey of Canada (Open File 6664).

Oldenburg, D., Li, Y., 1999. Estimating depth of investigation in DC resistivity and IP surveys. Geophysics 64, 403–416. http://dx.doi.org/10.1190/1.1444545.

Oldenborger, G.A., Pugin, A.J.-M., Pullan, S.E., 2013. Airborne time-domain electromagnetics, electrical resistivity and seismic reflection for regional three-dimensional mapping and characterization of the Spiritwood Valley Aquifer, Manitoba, Canada. Near Surf. Geophys. 11, 63–74. http://dx.doi.org/10.3997/1873-0604.2012023.

Paine, J.G., Minty, B.R.S., 2005. Airborne hydrogeophysics. Hydrogeoph. 50, 333–357. http://dx.doi.org/10.1007/1-4020-3102-5_11.

Podgorski, J.E., Auken, E., Schamper, C., Christiansen, A.V., Kalscheuer, T., Green, A.G., 2013. Processing and inversion of commercial helicopter time-domain electromagnetic data for environmental assessments and geologic and hydrologic mapping. Geophysics 78, 149–159. http://dx.doi.org/10.1190/GEO2012-0452.1.

Pugin, A.J.-M., Pullan, S.E., Hunter, J.A., Oldenborger, G.A., 2009. Hydrogeological prospecting using P and S-wave landstreamer seismic reflection methods. Near Surf. Geophys. 7, 315–327. http://dx.doi.org/10.3997/1873-0604.2009033.

Pugin, A.J.-M., Oldenborger, G.A., Pullan, S., 2011. Buried Valley imaging using 3-C seismic reflection, electrical resistivity and AEM surveys. 24th Symposium on the Application of Geophysics to Engineering and Environmental Problems (SAGEEP),Charleston, South Carolina, USA.

Raiche, A.P., Jupp, D.L.B., Rutter, H., Vozoff, K., 1985. The joint use of coincident loop transient electromagnetic and Schlumberger sounding to resolve layered structures. Geophysics 50, 1618–1627. http://dx.doi.org/10.1190/1.1441851.

Randich, P.G., Kuzniar, R.L., 1984. Geology of Towner County, North Dakota. North Dakota State Water Commission, County Groundwater Studies 36, Part III.

Sapia, V., Viezzoli, A., Jørgensen, F., Oldenborger, G.A., Marchetti, M., 2014. The impact on geological and hydrogeological mapping results of moving from ground to Airborne TEM. J. Env. Eng. Geoph 19, 53–66. http://dx.doi.org/10.2113/JEEG19.1.53.

Siemon, B., Kerner, T., Krause, Y., Noell, U., 2012. Airborne and ground geophysical investigation of the abandoned salt mine environment along the Stassfurt-Egeln Anticline, Germany. First Break 30, 43–53. http://dx.doi.org/10.3997/1365-2397.2011038.

Smith, R.S., Koch, R., Hodges, G., Lemieux, J., 2011. A comparison of airborne electromagnetic data with ground resistivity data over the Midwest deposit in the Athabasca basin. Near Surf. Geophys. 9, 319–330. http://dx.doi.org/10.3997/1873-0604.2011002.

Sørensen, K., Auken, E., 2004. SkyTEM—a new high-resolution helicopter transient electromagnetic system. Explor. Geophys. 35, 191–199. http://dx.doi.org/10.1071/EG04194.

Sørensen, K., Nyboe, N.S., 2012. Near surface resolution and turnoff times in airborne TEM investigations. Symposium on the Application of Geophysics to Environmental and Engineering Problems. Environmental and Engineering Geophysical Society.

Sutinen, R., Jakonen, M., Piekkari, M., Haavikko, P., Närhi, P., Middleton, M., 2010. Electrical-sedimentary anisotropy of Rogen moraine, Lake Rogen area, Sweden. Sediment. Geol. 232, 181–189.

Viezzoli, A., Christiansen, A.V., Auken, E., Sørensen, K., 2008. Quasi-3D modeling of airborne TEM data by spatially constrained inversion. Geophysics 73, 105–113. http://dx.doi.org/10.1190/1.2895521.

Viezzoli, A., Tosi, L., Teatini, P., Silvestri, S., 2010. Surface water–groundwater exchange in transitional coastal environments by airborne electromagnetics: the Venice Lagoon example. Geophys. Res. Lett. 37. http://dx.doi.org/10.1029/2009GL041572 (L01402).

Wiecek, S., 2009. Municipality of Killarney, Turtle Mountain groundwater assessment study. W.L. Gibbons & Associates Inc.

Winter, T.C., Benson, R.D., Engberg, R.A., Wiche, G.J., Emerson, D.G., Crosby, O.A., Miller, J.E., 1984. Synopsis of ground-water and surface-water resources of North Dakota. United States Geological Survey (Open File Report 84–732).

Wynn, J., 2002. Evaluating groundwater in arid lands using airborne magnetic/EM methods. An example in the southwestern U.S. and northern Mexico. Lead. Edge 21, 62–64. http://dx.doi.org/10.1190/1.1445851.